

## Porous nematic microfluidics for generation of umbilic defects and umbilic defect lattices

Jure Aplinc,<sup>1</sup> Stephen Morris,<sup>2</sup> and Miha Ravnik<sup>1,3,\*</sup>

<sup>1</sup>*Faculty of Mathematics and Physics, University of Ljubljana, Jadranska 19, 1000 Ljubljana, Slovenia*

<sup>2</sup>*Department of Engineering Science, University of Oxford, Parks Road, Oxford OX1 3PJ, United Kingdom*

<sup>3</sup>*Jozef Stefan Institute, Jamova 39, 1000 Ljubljana, Slovenia*

(Received 12 January 2016; revised manuscript received 29 March 2016; published 28 June 2016)

We demonstrate that porous nematic microfluidics is a potential route for the generation of nematic umbilic defects and regular umbilic defect lattices. By using numerical modeling we show that the mutual (backflow) coupling between the flow velocity and the orientation director field of the nematic liquid crystal leads to the formation of positive umbilic defects at local peaks and to the formation of negative umbilic defects at the local saddles in the flow profile. The number of flow peaks and the index of the flow saddles (i.e., the number of the valleys) are shown to be directly related to the strength of the umbilic defect, effectively relating the two fields at the geometrical level. The regular arrangement of the barriers in the porous channels is demonstrated to lead to the formation of regular lattices of umbilic defects, including square, triangular, and even kagome lattices. Experimental realization of such systems is discussed, with particular focus on microfluidic-tunable birefringent photonic band structures and lattices.

DOI: [10.1103/PhysRevFluids.1.023303](https://doi.org/10.1103/PhysRevFluids.1.023303)

### I. INTRODUCTION

Microfluidics considers the flow of fluids in submillimeter-size systems and typically under the influence of external forces [1]. The interest in microfluidics grew strongly in the past couple of decades because of the rapid evolution of laboratory-on-a-chip systems [1,2], which are 1000 times smaller than laboratory setups and are able to deal with very small volumes (1 nL or 1 pL) of samples [1]. At these volume scales, the typical volume forces (such as gravity and inertia), which are prominent in our daily life, generally become less important and instead forces such as surface tension and shear stress become dominant. The Reynolds number  $Re$  is generally small at these scales, so the fluid flow is in the laminar regime [3,4].

In addition to simple isotropic fluids, there is considerable fundamental and applied interest in the microfluidics of complex liquid crystalline fluids, as the internal structures of the fluid allow for novel mechanisms of manipulation, driving, and steering [5–12]. Nematic liquid crystals are best known for their technological use in display devices, but are at the modern state-of-the-art level also capable of forming ferromagnetic fluids [13,14], driving the colloidal self-assembly [15–18], transporting particles along topological defect lines [19], and manipulating the flow of light at the microscopic level [20,21]. The distinction of nematic liquid crystals from isotropic fluids lies in the orientational ordering of liquid crystal molecules caused by their anisotropic shape. This anisotropy notably affects also the flow of nematic liquid crystals, where the coupling between the (material) flow and the orientational order is called the backflow [22]. In the presence of flow velocity gradients, the backflow coupling causes the reorientation of the nematic director, i.e., it changes the average molecular orientation field. Typically, regimes of the rotating director (flow tumbling regime) or steady-state director with a fixed angle between the director and flow gradient (flow aligning regime) are observed [23].

---

\*miha.ravnik@fmf.uni-lj.si

The lowest-free-energy state of a (nonflowing) nematic is a homogeneous director field with a uniform nematic degree of order. However, in most cases, such a configuration is not compatible with the boundary conditions imposed by the surfaces or the external fields and the orientational order is frustrated. This frustration leads to formation of discontinuities in the director field, which are called defects [24–31]. Molecular orientation in the defect cores fluctuates rapidly and on average does not have a preferable direction of orientation. The vortexlike defects have accompanied liquid crystals since their discovery by Lehmann [32]; they are present also in a variety of fields of physics. Vortices attract a great deal of attention because of their universal character, as they are solutions of the complex Ginzburg-Landau equation [33–35] that describes different systems such as fluids, superfluids [36], superconductors, fluidized anisotropic granular matter, optical dielectrics, magnetic media, and strings from the field theory [33–35]. Defects are found even in light polarization singularities [37–39] and gravitational lensing shear fields [40]. In particular, defects in liquid crystals have proved to be a useful laboratory tool for studying defect behavior in cosmology [41].

In contrast with the conventional defects in liquid crystals, with a discontinuity at the center, umbilic defects have a continuous core and the discontinuity emerges only in the *projection* of the director field to a distinct plane perpendicular to the far field orientation [42]. These defects are also often interpreted as integer defects that have escaped in the third dimension. Liquid crystal umbilic defects are generally created by proper selection of anchoring, topology [43], applied electric [34,42,44–49] or magnetic fields [50,51], and even light pulses [52,53]. Recently, generation of umbilics by a Poiseuille flow was demonstrated [50,51] and the anisotropic annihilation dynamics of umbilic defects was studied [54,55]. It is important to note that today major attention is given to *singular* (i.e., not umbilic) topological defects, which were shown to form knots, links, and accompany complex-shaped colloidal particles, but much less attention is given to umbilics. The likely reasons are that (i) they are not fundamentally topological (i.e., they can be continuously transformed into a homogeneous field) and (ii) they are not simple to generate and stabilize. However, the ability to spontaneously generate umbilic defects in a controlled manner would be particularly interesting in the development of advanced photonic materials that consist of a defect site within a well-defined periodic structure. The presence of this defect site leads to a so-called defect mode that can enable either the propagation or trapping of light in an otherwise forbidden band. Unlike the conventional topological defects that are observed in liquid crystals, these umbilic defects may enable extended light propagation through a structure and lead to other interesting optical phenomena not observed with their topological counterparts. Furthermore, through the creation of a lattice of umbilic defects it may be possible to create a photonic lattice of defects. The idea of this paper is to show that umbilics can emerge naturally as steady-state structures in complex fluids and are actually elementary objects to emerge as a result of backflow coupling between the leading nonsingular nematic orientational order and the general flow profile characterized by multiple flow peaks and flow saddles.

In this paper we demonstrate backflow driven formation of umbilic (nonsingular) defects and regular defect arrays within porous nematic microfluidic channels using numerical modeling. Umbilic defects of various strengths are controllably generated by setting different complex flow profiles that distinctly include peak and saddle points. Umbilics of positive umbilic strength are found to emerge from multippeak flow profiles, with the number of flow peaks directly corresponding to the umbilic strength. Alternatively, umbilic defects of negative umbilic strength are found to emerge from saddle points in the flow profile, with the number of the valleys of the saddle (i.e. the index of the saddle) determining the umbilic strength. By introducing microchannels with regular porosity, we demonstrate the formation of various umbilic defect lattices, notably including also the kagome lattice, which is an indication of the conceptual diversity of umbilic defect states that can be generated in such porous systems via the proposed microfluidic approach. Experimental realization of umbilic states is outlined, with particular focus on the application of umbilic defect lattices as photonic elements, i.e., microfluidic tunable photonic crystals, where the effective dielectric constant of such microfluidics-generated photonic crystal could be tuned by the magnitude of the flow. Finally, the proposed work is an approach towards topology conditioned microfluidics and microrheology.

## II. METHODS AND MODELING

A strong approach for exploring the dynamics of nematic complex fluids and the related dynamic nematic structures is numerical modeling based on the Berris-Edwards model of nematodynamics [56]. Such an approach can explore a wide phase space and gives good qualitative or even quantitative agreement with experiments. Within the Berris-Edwards model the orientational order of the nematic liquid crystal is characterized by a symmetric and traceless order parameter tensor  $Q_{ij}$  and the flow of the nematic is described by the velocity flow field  $u_i$  and density  $\rho$ . Time-evolution equations for the mutually (backflow) coupled orientational field and material flow are given as

$$(\partial_t + u_k \partial_k) Q_{ij} - S_{ij} = \Gamma H_{ij}, \quad (1)$$

$$\rho(\partial_t + u_k \partial_k) u_i = \partial_j \Pi_{ij} + \eta \partial_j [\partial_i u_j + \partial_j u_i + (1 - 3\partial_\rho P) \partial_k u_k \delta_{ij}], \quad (2)$$

where  $\partial_t$  is the derivative in time,  $\partial_i$  is the derivative in the Cartesian spatial coordinate  $(x, y, z)$ ,  $\Gamma$  is the liquid crystal rotational diffusion coefficient,  $\eta$  is the viscosity, and  $\Pi_{ij}$  is the stress tensor

$$\begin{aligned} \Pi_{ij} = & -P\delta_{ij} + 2\xi(Q_{ij} + \delta_{ij}/3)(Q_{kl}H_{lk}) - \xi H_{ik}(Q_{kj} + \delta_{kj}/3) - \xi(Q_{ik} + \delta_{ik}/3)H_{kj} \\ & - \partial_i Q_{kl} \frac{\delta \mathcal{F}}{\delta \partial_j Q_{lk}} + Q_{ik}H_{kj} - H_{ik}Q_{kj}, \end{aligned} \quad (3)$$

where the parameter  $\xi$  depends on the molecular details of a given liquid crystal. Summation over repeated indices is assumed. The relaxation to equilibrium of  $Q_{ij}$  is determined by the molecular field  $H_{ij}$ , which originates from the equilibrium free energy  $\mathcal{F}$  of an elastic anisotropic fluid,  $H_{ij} = -\frac{\delta \mathcal{F}}{\delta Q_{ij}} + \text{Tr} \frac{\delta \mathcal{F}}{\delta Q_{kl}} \delta_{ij}/3$ , where

$$\mathcal{F} = \int_V [L(\partial_k Q_{ij})^2/2 + A Q_{ij} Q_{ji}/2 + B Q_{ij} Q_{jk} Q_{ki}/3 + C(Q_{ij} Q_{ji})^2/4] dV, \quad (4)$$

with  $L$  a single nematic elastic constant and  $A$ ,  $B$ , and  $C$  material constants. The advection term  $S_{ij}$  and effective compressibility term are defined as

$$S_{ij} = (\xi D_{ik} + \Omega_{ik})(Q_{kj} + S\delta_{kj}/2) + (Q_{ik} + S\delta_{ik}/2)(\xi D_{kj} - \Omega_{kj}) - 2\xi(Q_{ij} + S\delta_{ij}/2)(Q_{kl}\partial_k u_l), \quad (5)$$

$$P = P_0\rho - L(\partial_k Q_{ij})^2/2, \quad (6)$$

where  $D_{ij} = (\partial_j u_i + \partial_i u_j)/2$ ,  $\Omega_{ij} = (\partial_j u_i - \partial_i u_j)/2$ , and  $P_0$  is the hydrostatic pressure.

We solve the dynamic equations for the flow  $u_i$  and the orientational order parameter  $Q_{ij}$  by using the hybrid lattice Boltzmann algorithm [6,57,58]. The time evolution for  $Q_{ij}$  is calculated by using the finite-difference scheme in time, whereas the equation for  $u_i$  is solved by the D3Q15 lattice Boltzmann method [58]. The simulations are performed in a slice through the microchannel with a cubic lattice, typically  $200 \times 200 \times 30$  mesh points. Along the channel  $z$ , we assume periodic boundary conditions for both  $Q_{ij}$  and  $u_i$ , whereas at the channel walls we take no-slip boundary conditions for  $u_i$  and fixed in-plane boundary conditions for  $Q_{ij}$ . Unless otherwise stated, the following values for material parameters are used:  $L = 40$  pN,  $A = -0.172$  MJ/m<sup>3</sup>,  $B = -2.12$  MJ/m<sup>3</sup>,  $C = 1.73$  MJ/m<sup>3</sup>,  $\xi = 0.6$ ,  $P_0 = 100$  kPa,  $\Gamma = 7.29$  Pa s, mesh resolution  $\Delta x = 10$  nm, time step  $\Delta t = 0.34$   $\mu$ s, and body force  $f = 0.01$   $\rho \Delta x / \Delta t^2$ .

## III. GEOMETRY-CONDITIONED NEMATIC MICROCHANNELS

The geometrical cross section is the elementary variability of channels in microfluidic setups. Therefore, it is the natural first step in understanding the role of geometrical confinement in porous microfluidics, which effectively can be considered as if consisting of multiple subregions of various geometries and cross sections. Figures 1(a)–1(d) show the flow of nematic fluid pushed by a constant

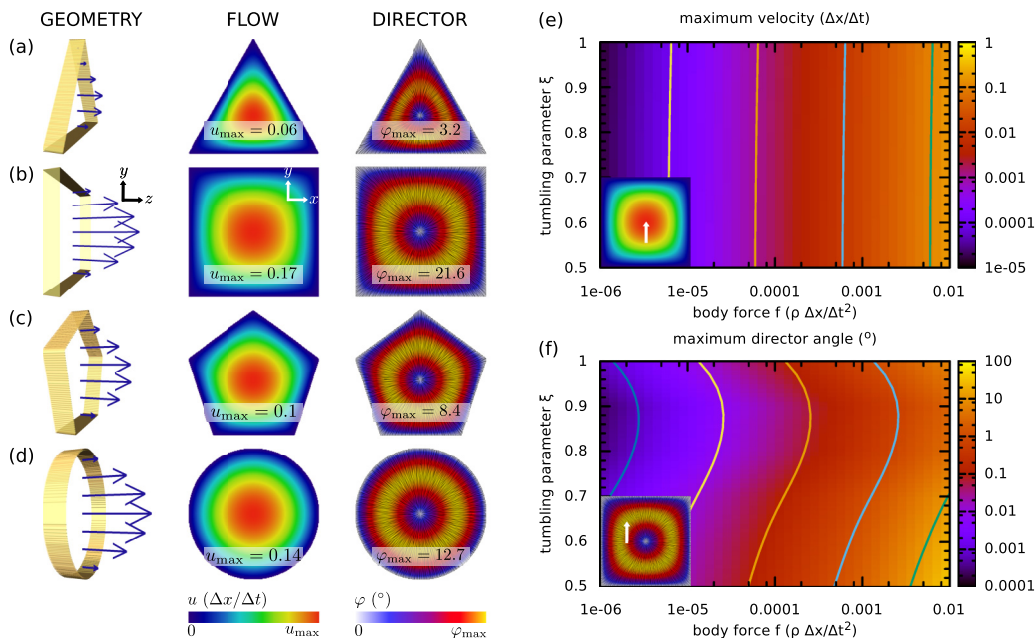


FIG. 1. Nematic liquid crystal flow in microchannels of different geometries driven with constant body force. (a)–(d) Flow velocity and director deformation fields (angle between director and channel axis  $z$ ) are indicated with colors: Gray and white streamlines show the projection of the director on the  $xy$  plane. Strong homogeneous planar anchoring in the direction of the channel axis  $z$  is imposed at the channel surfaces. The body force  $f = 1 \times 10^{-2} \rho \Delta x / \Delta t^2$ . (e) Maximum velocity and (f) director deformation in a square channel (location in the channel indicated with the white arrow) as functions of tumbling parameter  $\xi$  and body force  $f$ .

body force along microchannels of different geometries, with surfaces imposing homogeneous alignment of the director along the channel axis  $z$ . The flow profile near the channel wall responds to the geometry of the channel, but becomes more circular-tube-like in the center of the channel. In contrast, the nematic profile starts to deviate from the homogeneous alignment imposed by the walls because of the coupling with the flow field (shear profile) in the central region of the channel [see Figs. 1(a)–1(d)] and can be interpreted as a +1 umbilic defect. Notably, the director has no singular region, but is everywhere continuous and can be, from the standpoint of topology, virtually continuously transformed into a homogeneous field. The umbilic defect-type field profile emerges in the *projection* of the director onto the plane perpendicular to the general director alignment direction ( $z$  axis), i.e., in the cross section of the channel [26,42]. The profile in this projected director also determines the strength (effectively, the winding number) of umbilic defects. The director deformation of the umbilic can be locally measured with the angle between the deviated director and the axis  $z$  and is shown with colors in the right column of Figs. 1(a)–1(d). Maximum values of the flow velocity and director deformation both depend on the microchannel geometry and surface of the channel cross section. For channels with equal cross-section area, the maximum flow velocity and maximum director deformation emerge in a circular microchannel and decrease with the number of edges.

In order to maximize the backflow coupling between the flow and nematic director, i.e., make umbilic defects more pronounced by maximizing the  $xy$  projection component of the nematic director, we vary the two key parameters of the system: (i) the body force driving the flow and (ii) the material parameter  $\xi$ , which depends on the molecular properties of the liquid crystal [26,59]. Figure 1(e) shows the maximum velocity (reached in the center of the microchannel) and Fig. 1(f) the maximum deformation of the director field (reached at the tip of the arrow depicted in the inset)

as a function of tumbling parameter  $\xi$  and body force  $f$  for a square channel. Within a given channel, the maximum velocity proves to be in a broad range of values linearly dependent on the body force  $f$  and weakly varies with the tumbling parameter  $\xi$  [Fig. 1(e)]. Both the maximum velocity and director deformation are highest in the regime  $\xi \sim 0.5$  [Fig. 1(f)]. The maximum angle of director deformation from the homogeneous configuration has a minimum at  $\xi \sim 0.9$ , where it drops for more than an order of magnitude. All the following simulations presented here are done at  $\xi = 0.6$ .

In terms of potential experiments to demonstrate the formation of these umbilic defects in the different geometries, a microfluidic device comprising a combination of cylindrical and rectangular capillaries would be required whereby the flow rate of the nematic is controlled by a syringe pump. These barriers could be pinned mutually and to the channel walls at some (large) distances, generating long regions of microchannels with effectively separate long cylindrical barriers that create regular pores. An optical polarizing microscope and a high speed camera could then be used to monitor the formation and behavior of the umbilic defects.

#### IV. POROUS NEMATIC MICROCHANNELS

Umbilic defects are observed to emerge when the nematic is pushed along the porous microchannels. The porous channels are set up as rectangular microchannels with inserted cylindrical barriers, e.g., visualize long cylindrical fibers immersed in the channels (Fig. 2). The introduced barriers (i) increase the surface area where the flow velocity is imposed to be zero and (ii) decrease the fraction of the channel cross section accessible to the fluid, i.e., decrease the porosity of the channel. Consequently, both the flow velocity and director deformation diminish when the porosity of the microchannel is decreased. However, more importantly, the porous barriers change the effective landscape of the microfluidic channel by introducing geometrical pores of various shapes and sizes, which cause the flow velocity to obtain multiple flow peaks and flow saddle points [Fig. 2(e)]. Effectively, both the material flow and the nematic distortion become locally compartmentalized by the pores into effective channel-like regions of different geometries. Further, it is the local flow peaks and saddles within such effective channel-like regions that generate the umbilic defects via the backflow mechanism [Fig. 2(e)].

Figures 2(a)–2(c) shows the square microfluidic channel with one inserted cylindrical barrier. As the radius of the barrier is increased, the four maxima in the flow velocity become localized and flow saddle points between them become more pronounced. A similar phenomenon is observed in the case of two [Figs. 2(d) and 2(e)] and four [Figs. 2(f) and 2(g)] barriers in the microchannel, generating different configurations of the local flow peaks and flow saddles. In such channels, the deformation of the director field is a result of competition between the surface alignment imposed by the channel surfaces and the flow shear, where the flow shear turns the director away from the direction imposed by the surfaces. We observe that a local maximum in the flow field yields an umbilic defect of strength  $+1$  and a simple index-2 saddle point gives an umbilic defect of strength  $-1$  [insets to Fig. 2(e)]. The director field in the umbilic defect is tilted relative to its core and is consequently continuous everywhere in space. A notable difference between regular defects in liquid crystals, called disclinations, and umbilic defects is that half integer (winding number) defect lines can occur in disclinations, but not in umbilic defect lines. Therefore, umbilics of strengths  $+1$  and  $-1$ , which occur in our porous microchannels, are expectedly the lower elastic energy deformations.

The flow field in porous microfluidic channels was shaped by cylindrical barriers and only the two simplest flow profiles, i.e., flow peaks and flow saddles, emerged, which gave umbilic defects of strengths  $+1$  and  $-1$ . However, by designing flow profiles with different symmetry beyond simple peaks and saddles, umbilic defects of higher umbilic strength can be created. We perform simulations in an (empty) square microchannel with a predefined and fixed velocity profile of distinct symmetry and calculate the nematic orientation for such imposed shear flow. Expectedly, a peak in the velocity field generates a  $+1$  umbilic and a saddle a  $-1$  umbilic (Fig. 3). Two peaks without a saddle point (a minimum and a maximum) generate an umbilic of strength  $+2$ , whereas a three-valley (index 3)

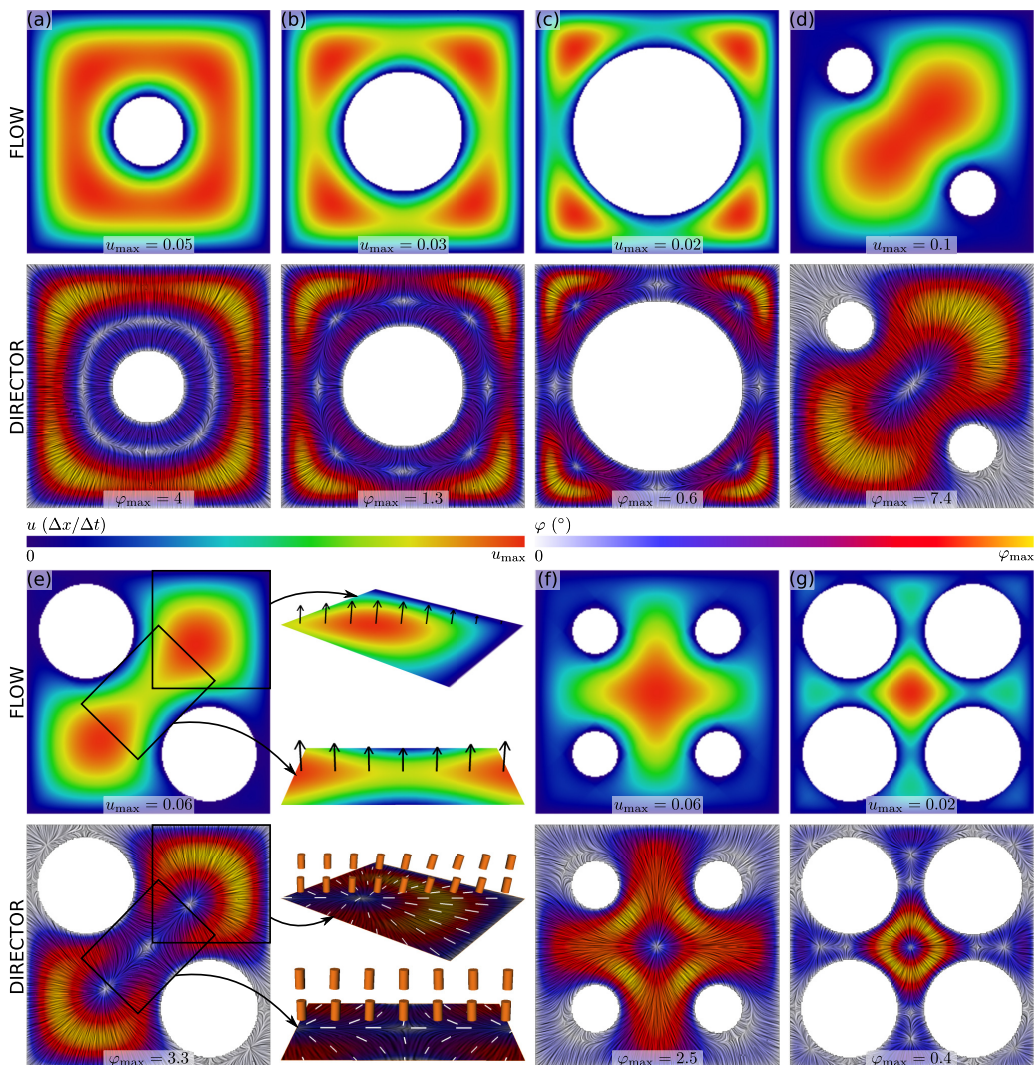


FIG. 2. Flow and director profiles in porous microchannels with (a)–(c) one, (d) and (e) two, and (f) and (g) four cylindrical barriers. Umbilic defects in the director field of umbilic strength  $+1$  emerge at local flow peaks (i.e., local maximum or minimum) and umbilic defects of umbilic strength  $-1$  emerge in the flow saddle point.

saddle and a four-valley (index 4) saddle yield umbilics of strength  $-2$  and  $-3$ , respectively. As shown in Fig. 3, in a local core region, the  $-3$  umbilic can decompose into one  $+1$  umbilic defect and four  $-1$  umbilics, keeping the umbilic strength conserved.

The direct relation between the shape of the local flow profile and the generation of umbilic defects of various umbilic strengths can be shown also by simple analytical calculations. If one assumes incompressible nematic fluid and a constant nematic degree of order ( $S = \text{const}$ ) and takes the director  $\mathbf{n}$  instead of the order parameter tensor  $\mathbf{Q}$  for the hydrodynamic variable [i.e., assuming the uniaxial order parameter tensor  $Q_{ij} = S(3n_i n_j - \delta_{ij})/2$ ], the Berris-Edwards model reduces to the Ericksen-Leslie hydrodynamic theory of nematic liquid crystals [25,26]. The time-evolution equation for  $Q_{ij}$  [Eq. (1)] reduces to the director equation [25]

$$I \frac{d}{dt} [\mathbf{n} \times \dot{\mathbf{n}}] = \mathbf{n} \times \mathbf{H} + \mathbf{\Gamma}, \quad (7)$$

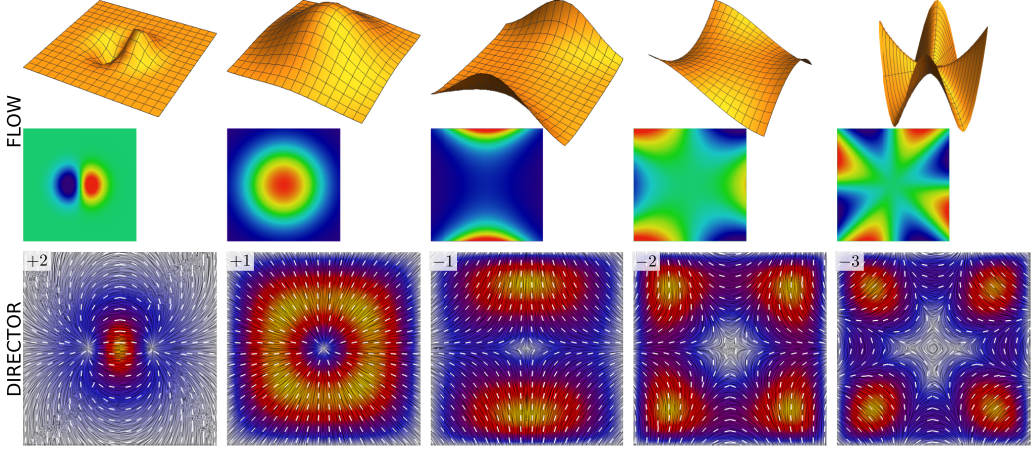


FIG. 3. Generation of umbilic defects of variable (high) umbilic strength. A local peak in the velocity field generates a +1 umbilic and two peaks of different signs generate +2 umbilic. Umbilics of negative signs (−1, −2, and −3) are generated if the velocity field has a saddle point with two, three, and four valleys, respectively. In the core region, the −3 umbilic can decompose into one +1 umbilic and four −1 umbilics.

where  $I$  is the moment of inertia per unit volume,  $\mathbf{\Gamma} = -\gamma_1[\mathbf{n} \times \mathbf{N}] - \gamma_2[\mathbf{n} \times \mathbf{D} \cdot \mathbf{n}]$  is the viscous torque,  $\mathbf{N} = \dot{\mathbf{n}} - \boldsymbol{\omega} \times \mathbf{n}$  describes relative rotations of the director, and  $\gamma_1 = \alpha_3 - \alpha_2 > 0$  and  $\gamma_2 = \alpha_6 - \alpha_5 = \alpha_2 + \alpha_3$  are combinations of Leslie viscosities. At low-frequency excitations, the inertia term can be neglected and Eq. (7) reduces to

$$\mathbf{n} \times \mathbf{H} = \mathbf{n} \times (\gamma_1 \mathbf{N} + \gamma_2 \mathbf{D} \cdot \mathbf{n}), \quad (8)$$

which gives the connection between the nematic molecular field  $\mathbf{H}$  and the velocity gradient tensor  $\mathbf{D}$ :

$$\mathbf{H} = -\gamma_1 \boldsymbol{\omega} \times \mathbf{n} + \gamma_2 \mathbf{D} \cdot \mathbf{n}. \quad (9)$$

The latter coupling in Eq. (9) between the nematic director and the material flow shows that by imposing a distinct velocity profile, one can control the molecular field, i.e., the equilibrium alignment of the nematic.

We take a two-dimensional (2D) Gaussian function (−) and a 2D Gaussian index-2 saddle (+) to resemble a local peak and a saddle in the velocity profile [60]

$$\mathbf{u}(x, y) = a \exp\left(-\frac{x^2}{2c^2} \mp \frac{y^2}{2c^2}\right) \mathbf{e}_z, \quad (10)$$

where the parameter  $a$  determines the height of the function peak and  $c$  (the standard deviation) controls the width of the Gaussian peak. We calculate the velocity gradient tensor  $D_{ij}$  using predefined profiles (10), which yields the corresponding molecular field

$$\mathbf{H} = \gamma_1 \boldsymbol{\omega} \times \mathbf{n} + \frac{1}{2c^2} \gamma_2 u_z(x, y) \begin{pmatrix} -xn_z \\ \mp yn_z \\ -xn_x \mp yn_y \end{pmatrix}. \quad (11)$$

Indeed, for the Gaussian velocity profile, the corresponding molecular field has rotational symmetry around the  $z$  axis, whereas for the Gaussian saddle-shaped velocity profile, the corresponding normalized molecular field has a  $C_4$  symmetry, which corresponds to the symmetry of the −1 umbilic. In equilibrium, the director must be at each point parallel to the molecular field [26]. Furthermore, if normalizing the molecular fields calculated from the Gaussian saddle velocity field

in the  $xy$  plane for visualization reasons, they show a profile similar to the director profiles of umbilic defects projected on the  $xy$  plane. So the symmetry and the shape of the normalized molecular field equal the symmetry of the outgoing umbilic defects. Such a simplified Ericksen-Leslie analytical approach works well also for umbilics of higher strengths, reproducing the symmetry and roughly the projection of their director profile.

## V. MICROCHANNELS WITH REGULAR POROSITY AS GENERATORS OF UMBILIC LATTICES

With the knowledge of mutual coupling between the flow profiles and nematic orientation, different regular and irregular configurations of umbilic defects can be created, notably including diverse umbilic defect lattices. We use rectangular microfluidic channels and impose porosity with cylindrical barriers arranged in three regular configurations: triangular, square, and hexagonal lattices. Generally, we observe that the flow field in such microchannels with cylindrical barriers has locally only two basic profiles, namely, local peaks or local index-2 saddles (Fig. 4), which generate the basic  $\pm 1$

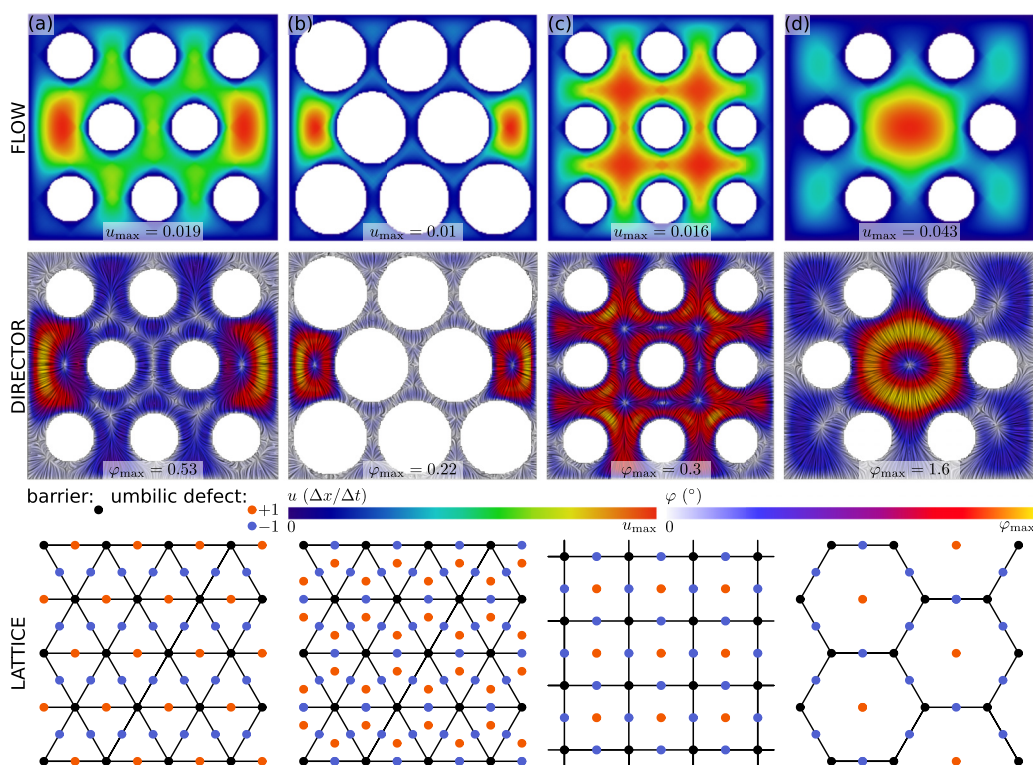


FIG. 4. Porous nematic microchannels as generators of umbilic defect lattices. Porous microchannels with cylindrical barriers are arranged into (a) and (b) triangular, (c) square, and (d) hexagonal lattices. The triangular lattice of barriers (a) and (b) can generate two possible lattices of the umbilics, depending on the diameter of the cylindrical barriers. In the thin cylinders regime (a), a triangular lattice of  $+1$  umbilics and a rectangular lattice of  $-1$  umbilics form. In the thick cylinders regime (b), a hexagonal lattice of  $+1$  umbilics and a kagome lattice of  $-1$  umbilics form. (c) For the square lattice of barriers, both types of umbilics form square lattices. (d) For the hexagonal lattice of barriers,  $+1$  umbilics form a triangular lattice and  $-1$  umbilics form a kagome lattice. The bottom panels show generalization of the observed umbilic patterns from finite-size channels to the (infinite) periodic umbilic lattice structure; black dots indicate barrier positions, orange dots show  $+1$ , and blue dots show  $-1$  umbilic defects.

umbilic defects. Performing the study in finite-size channels, the flow field is affected by the confining microchannel walls, where surface effects can distort and affect the lattice of the umbilics.

Figures 4(a) and 4(b) shows the microchannel with a triangular lattice of barriers where, depending on the barrier radius, we observe the formation of two different lattices of the umbilic defects. In the thin barrier regime,  $+1$  umbilics form a triangular lattice and  $-1$  umbilics a square lattice. However, if the barriers are thick compared to the interspaces between them,  $+1$  umbilics form a hexagonal lattice and  $-1$  umbilics arrange into a kagome lattice. Both types of umbilic defects in a porous microchannel with a square lattice of barriers [Fig. 4(c)] form lattices of the same symmetry. If the barriers are arranged into a hexagonal lattice [Fig. 4(d)], umbilic defects of strength  $+1$  form a triangular lattice and  $-1$  umbilics form a kagome lattice.

To generalize the results, the mutual (backflow) coupling between the flow field and nematic orientational ordering is shown in an interesting way for creating birefringent defect lattices in complex fluids via a direct microfluidic approach. By controlling the symmetry and size of the porous barriers in the channels, one can design various umbilic arrangements and lattices ranging from simple square to triangular and even kagome. As objects, the umbilic defects are inherently birefringent and could be used for manipulating the flow of light at various levels and frequency scales, depending on the pore (barrier) design and size. Also, umbilic defects could be used as switchable and controllable objects for trapping and guiding inclusions, such as colloidal particles, in the microchannels, relevant in the fields of microtransport and mixing. By further designing and changing the surface conditions at the porous barriers (e.g., making the surfaces impose homeotropic anchoring), the formation of umbilic defects could be complemented also by the emergence of singular defects (such as  $+1/2$  and  $-1/2$  disclination lines), which would add a further variability to the material.

Creating the umbilic defect lattices from an experimental point of view is by no means trivial. However, we propose that this may be achieved using direct laser writing to create cylindrical polymer channels in a nematic liquid crystal device that consists of reactive mesogens and a photoinitiator. With the use of two-photon polymerization it should be possible to create well defined polymer cylinders that are located at precise positions within the device. Furthermore, with the use of adaptive optics it should also be possible to form the structures *in situ* and with the aid of a spatial light modulator an array of these cylinders in any one of the potential configurations (i.e., square, triangular, or hexagonal) could be created. To induce flow, a piezoelectric transducer would be connected to the nematic liquid crystal device.

Cylindrical barriers may have a different refractive index than the surrounding liquid crystal, which is birefringent and given by the director orientation. Regular lattices of barriers and umbilic defects of different symmetries thus form complex composite birefringent photonic crystal materials, where one contribution to the band structure is determined by the 2D periodic lattice of umbilic defects and the second contribution emerges from the regular lattice of the cylindrical barriers. Flow rate and the barrier size, besides the material constants, are direct parameters that could be used to tune the optical bands and band gaps of these photonic materials as they affect the effective dielectric contrast of the photonic crystal. We should comment that the effects of bulk heating are generally small in such complex liquid crystal geometries, where the aimed effects come from the heating via surfaces [61]. More generally, such photonic crystal materials may offer an alternative, microfluidics-based approach towards tunable soft matter photonic materials. Additional interesting variability of these materials could become available by also applying external fields, including electric and magnetic.

## VI. CONCLUSION

We introduced porous nematic microfluidics as a controllable system for generating complex regular configurations of nematic umbilic defects, ranging from individual umbilics to umbilic lattices, such as square, triangular, and even kagome lattices. With their complex spatial variation of birefringence, the generated porous umbilic systems are photonic materials of conceptually different design: Essentially, the umbilics produce optical lattices of *some* symmetry within the optical lattices of the barriers with *another* symmetry, which may be used as a route to tunable photonics based

on materials with inherently multiple underlying symmetries. Specifically, we performed hybrid lattice Boltzmann simulations of driven nematic liquid crystal flow in rectangular microchannels with inserted cylindrical barriers and also clearly discussed the experimental realization of such systems. The porous barriers inside the microfluidic channel change the effective landscape of the channel, creating narrow and wide regions for the flow to pass, which results in the formation of local peaks and saddles in the flow field, which in turn results in the formation of the umbilic defects, i.e., geometrically distinct spatial variations of birefringence. Umbilic defects of umbilic strength  $+1$  form at local flow peaks, whereas umbilics of umbilic strength  $-1$  emerge at simple index-2 saddle points. Furthermore, we showed that umbilics of higher umbilic strength can be formed via controlling the geometry of the flow velocity profile, which is an interesting generalization that provides direct insight into the actions of the backflow mechanism with relevance in various complex fluids, notably including active nematics. Finally, this work is an approach towards realizing microfluidically tunable optical and photonic materials and may find relevance in diverse systems with internal order, ranging from flexible polymers under shear to active fluids.

### ACKNOWLEDGMENTS

The authors thank S. Žumer and J. M. Yeomans for discussions on this topic and acknowledge funding from the Slovenian Research Agency ARRS, through Grants No. Z1-5441 and No. P1-0099, and EU FP7 Career Integration Grant FREEFLUID.

- 
- [1] H. Bruus, *Theoretical Microfluidics* (Oxford University Press, Oxford, 2011).
  - [2] C. A. Stan, L. Guglielmini, A. K. Ellerbee, D. Caviezel, H. A. Stone, and G. M. Whitesides, Sheathless hydrodynamic positioning of buoyant drops and bubbles inside microchannels, *Phys. Rev. E* **84**, 036302 (2011).
  - [3] J. de Jong, M. J. Geerken, R. G. H. Lammertink, and M. Wessling, Porous microfluidic devices – fabrication and applications, *Chem. Eng. Technol.* **30**, 309 (2007).
  - [4] P. Tabeling, *Introduction to Microfluidics* (Oxford University Press, Oxford, 2010).
  - [5] B. F. B. Silva, M. Zepeda-Rosales, N. Venkateswaran, B. J. Fletcher, L. G. Carter, T. Matsui, T. M. Weiss, J. Han, Y. Li, U. Olsson, and C. R. Safinya, Nematic director reorientation at solid and liquid interfaces under flow: SAXS studies in a microfluidic device, *Langmuir* **31**, 4361 (2015).
  - [6] A. Sengupta, U. Tkalec, M. Ravnik, J. M. Yeomans, C. Bahr, and S. Herminghaus, Liquid Crystal Microfluidics for Tunable Flow Shaping, *Phys. Rev. Lett.* **110**, 048303 (2013).
  - [7] M. Ravnik and J. M. Yeomans, Confined Active Nematic Flow in Cylindrical Capillaries, *Phys. Rev. Lett.* **110**, 026001 (2013).
  - [8] J. S. Lintuvuori, K. Stratford, M. E. Cates, and D. Marenduzzo, Colloids in Cholesterics: Size-Dependent Defects and Non-Stokesian Microrheology, *Phys. Rev. Lett.* **105**, 178302 (2010).
  - [9] A. Sengupta, S. Herminghaus, and C. Bahr, Liquid crystal microfluidics: Surface, elastic and viscous interactions at microscales, *Liq. Cryst.* **2**, 73 (2014).
  - [10] K. Stratford, O. Henrich, J. S. Lintuvuori, M. E. Cates, and D. Marenduzzo, Self-assembly of colloid-cholesteric composites provides a possible route to switchable optical materials, *Nat. Commun.* **5**, 3954 (2014).
  - [11] D. A. Beller, M. A. Gharbi, A. Honglawan, K. J. Stebe, S. Yang, and R. D. Kamien, Focal Conic Flower Textures at Curved Interfaces, *Phys. Rev. X* **3**, 041026 (2013).
  - [12] Y. Xia, F. Serra, R. D. Kamien, K. J. Stebe, and S. Yang, Direct mapping of local director field of nematic liquid crystals at the nanoscale, *Proc. Natl. Acad. Sci. USA* **112**, 15291 (2015).
  - [13] A. Mertelj, D. Lisjak, M. Drofenik, and M. Čopič, Ferromagnetism in suspensions of magnetic platelets in liquid crystal, *Nature (London)* **504**, 237 (2013).
  - [14] A. Mertelj, A. Rešetič, S. Gyergyek, D. Makovec, and M. Čopič, Anisotropic microrheological properties of chain-forming magnetic fluids, *Soft Matter* **7**, 125 (2011).

- [15] I Muševič, U Škarabot, M. Tkalec, M. Ravnik, and S. Žumer, Two-dimensional nematic colloidal crystals self-assembled by topological defects, *Science* **313**, 954 (2006).
- [16] M. B. Pandey, T. Porenta, J. Brewer, A. Burkart, S. Čopar, S. Žumer, and I. I. Smalyukh, Self-assembly of Skyrmion-dressed chiral nematic colloids with tangential anchoring, *Phys. Rev. E* **89**, 060502(R) (2014).
- [17] P. J. Ackerman, J. van de Lagemaat, and I. I. Smalyukh, Self-assembly and electrostriction of arrays and chains of hopfion particles in chiral liquid crystals, *Nat. Commun.* **6**, 6012 (2015).
- [18] F. E. Mackay and C. Denniston, Locally stable diamond colloidal crystal formed in a cholesteric liquid crystal, *Soft Matter* **10**, 4430 (2014).
- [19] A. Sengupta, Topological constraints in a microfluidic platform, *Liq. Cryst.* **41**, 290 (2014).
- [20] M. Humar, M. Ravnik, S. Pajk, and I. Muševič, Electrically tunable liquid crystal optical microresonators, *Nat. Photon.* **3**, 595 (2009).
- [21] M. Čančula, M. Ravnik, and S. Žumer, Generation of vector beams with liquid crystal disclination lines, *Phys. Rev. E* **90**, 022503 (2014).
- [22] J. L. Ericksen, Anisotropic fluids, *Arch. Ration. Mech. Anal.* **4**, 231 (1959).
- [23] G. Rienäcker, M. Kröger, and S. Hess, Chaotic orientational behavior of a nematic liquid crystal subjected to a steady shear flow, *Phys. Rev. E* **66**, 040702 (2002).
- [24] S. Chandrasekhar, *Liquid Crystals* (Cambridge University Press, Cambridge, 1992).
- [25] M. Kleman and O. D. Lavrentovich, *Soft Matter Physics: An Introduction* (Springer, New York, 2003).
- [26] P.-G. de Gennes and J. Prost, *The Physics of Liquid Crystals* (Oxford University Press, Oxford, 1993).
- [27] T. Stieger, S. Püschel-Schlotthauer, M. Schoen, and M. G. Mazza, Flow-induced deformation of closed disclination lines near a spherical colloid immersed in a nematic host phase, *Mol. Phys.* **114**, 259 (2015).
- [28] H. Stark and D. Ventzki, Stokes drag of spherical particles in a nematic environment at low Ericksen numbers, *Phys. Rev. E* **64**, 031711 (2001).
- [29] M. Tasinkevych, M. G. Campbell, and I. I. Smalyukh, Splitting, linking, knotting, and solitonic escape of topological defects in nematic drops with handles, *Proc. Natl. Acad. Sci. USA* **111**, 16268 (2014).
- [30] P. J. Ackerman, Z. Qi, Y. Lin, C. W. Twombly, M. J. Laviada, Y. Lansac, and I. I. Smalyukh, Laser-directed hierarchical assembly of liquid crystal defects and control of optical phase singularities, *Sci. Rep.* **2**, 414 (2012).
- [31] G. P. Alexander, B. G. Chen, E. A. Matsumoto, and R. D. Kamien, Colloquium: Disclination loops, point defects, and all that in nematic liquid crystals, *Rev. Mod. Phys.* **84**, 497 (2012).
- [32] O. Lehmann, Über fließende krystalle, *Z. Phys. Chem.* **4**, 462 (1889).
- [33] L. M. Pismen, *Vortices in Nonlinear Fields* (Clarendon, Oxford, 1999).
- [34] M. G. Clerc, E. Vidal-Henriquez, J. D. Davila, and M. Kowalczyk, Symmetry breaking of nematic umbilical defects through an amplitude equation, *Phys. Rev. E* **90**, 012507 (2014).
- [35] I. S. Aranson and L. Kramer, The world of complex ginzburg-landau equation, *Rev. Mod. Phys.* **74**, 99 (2002).
- [36] G. P. Bewley, M. S. Paoletti, K. R. Sreenivasan, and D. P. Lathrop, Characterisation of reconnecting vortices in superfluid helium, *Proc. Natl. Acad. Sci. USA* **105**, 13707 (2008).
- [37] F. Flossmann, K. O'Holleran, M. R. Dennis, and M. J. Padgett, Polarization Singularities in 2D and 3D Speckle Fields, *Phys. Rev. Lett.* **100**, 203902 (2008).
- [38] F. Cardano, E. Karimi, L. Marucci, C. de Lisio, and E. Santamato, Generation and dynamics of optical beams with polarization singularities, *Opt. Express* **21**, 8815 (2013).
- [39] V. Kumar and N. K. Viswanathan, Topological structures in vector-vortex beam fields, *J. Opt. Soc. Am. B* **31**, A40 (2014).
- [40] V. Vitelli, B. Jain, and R. D. Kamien, Topological defects in gravitational lensing shear fields, *J. Cosmol. Astropart. Phys.* **2009**, 034 (2009).
- [41] M. J. Bowick, L. Chandar, E. A. Schiff, and A. M. Srivastava, The cosmological Kibble mechanism in the laboratory: String formation in liquid crystals, *Science* **263**, 943 (1994).
- [42] A. Rapini, Umbilics: Static properties and shear-induced displacements, *J. Phys.* **34**, 629 (1973).
- [43] T. Machon and G. P. Alexander, Umbilic Lines in Orientational Order, *Phys. Rev. X* **6**, 011033 (2016).
- [44] A. Rapini, L. Léger, and A. Marinet, Umbilics: Static and dynamical properties, *J. Phys. (Paris) Colloq.* **36**, C1-189 (1975).

- [45] T. A. Kumar, V. S. S. Sastry, K. Ishikawa, H. Takezoe, N. V. Madhusudana, and S. Dhara, Effect of an electric field on defects in a nematic liquid crystal with variable surface anchoring, *Liq. Cryst.* **38**, 971 (2011).
- [46] J. G. Wei and S. H. Chen, Electric-field-induced director-field transition of nematic liquid crystal in a closed conical cavity, *Jpn. J. Appl. Phys.* **33**, 6249 (1994).
- [47] J. G. Wei and S. H. Chen, Stability of an umbilical director field of nematic liquid crystal in a closed conical cavity, *Jpn. J. Appl. Phys.* **33**, L660 (1994).
- [48] P. Kumar, U. S. Hiremath, C. V. Yelamaggad, A. G. Rossberg, and K. S. Krishnamurthy, Electroconvection in a homeotropic bent-rod nematic liquid crystal beyond the dielectric inversion frequency, *J. Phys. Chem. B* **112**, 9753 (2008).
- [49] I. I. Smalyukh, B. I. Senyuk, P. Palffy-Muhoray, O. D. Lavrentovich, H. Huang, E. C. Gartland, Jr., V. H. Bodnar, T. Kosa, and B. Taheri, Electric-field-induced nematic-cholesteric transition and three-dimensional director structures in homeotropic cells, *Phys. Rev. E* **72**, 061707 (2005).
- [50] P. Pieranski, B. Yang, L. J. Burtz, A. Camu, and F. Simonetti, Generation of umbilics by magnets and flows, *Liq. Cryst.* **40**, 1593 (2013).
- [51] P. Pieranski, Generation of umbilics by poiseuille flows, *Eur. Phys. J. E* **37**, 24 (2014).
- [52] R. Barboza, U. Bortolozzo, G. Assanto, E. Vidal-Henriquez, M. G. Clerc, and S. Residori, Vortex Induction via Anisotropy Stabilized Light-Matter Interaction, *Phys. Rev. Lett.* **109**, 143901 (2012).
- [53] R. Barboza, U. Bortolozzo, G. Assanto, E. Vidal-Henriquez, M. G. Clerc, and S. Residori, Harnessing Optical Vortex Lattices in Nematic Liquid Crystals, *Phys. Rev. Lett.* **111**, 093902 (2013).
- [54] I. Dierking, M. Ravnik, E. Lark, J. Healey, G. P. Alexander, and J. M. Yeomans, Anisotropy in annihilation dynamics of umbilic defects in nematic liquid crystal, *Phys. Rev. E* **85**, 021703 (2012).
- [55] I. Dierking, O. Marshall, J. Wright, and N. Bulleid, Annihilation dynamics of umbilical defects in nematic liquid crystals under applied electric fields, *Phys. Rev. E* **71**, 061709 (2005).
- [56] A. N. Beris and B. J. Edwards, *Thermodynamics of Flowing Systems: With Internal Microstructure* (Oxford University Press, New York, 1994).
- [57] D. Marenduzzo, E. Orlandini, M. E. Cates, and J. M. Yeomans, Steady-state hydrodynamic instabilities of active liquid crystals: Hybrid lattice Boltzmann simulations, *Phys. Rev. E* **76**, 031921 (2007).
- [58] C. Denniston, D. Marenduzzo, E. Orlandini, and J. M. Yeomans, Lattice Boltzmann algorithm for three-dimensional liquid-crystal hydrodynamics, *Philos. Trans. R. Soc. London* **362**, 1745 (2004).
- [59] S. A. Edwards and Y. M. Yeomans, Spontaneous flow states in active nematics: A unified picture, *Europhys. Lett.* **85**, 18008 (2009).
- [60] The Gaussian shape of the flow peak and saddle is used only for convenience in the calculations, as in realistic flow profiles the exact functional shape can be very different. However, as long as the general peak or saddle shape is retained, the mutual coupling between the flow and orientation generates the umbilic defects .
- [61] M. Škarabot, Ž. Lokar, and I. Mušević, Transport of particles by a thermally induced gradient of the order parameter in nematic liquid crystals, *Phys. Rev. E* **87**, 062501 (2013).